One-way wave-equation migration of compressional and converted waves in a VTI medium

Ørjan Pedersen*† and Bjørn Ursin* and Hans-Kristian Helgesen†*

ABSTRACT

In seismic reflection surveying, by recording both pressure and shear-wave reflections, one can increase the amount of information obtained about the subsurface than by recording pressure waves alone. Geologic structures which are not visible by using conventional pressure-data may possibly be imaged using shear waves, thus mitigating the risk in oil and gas exploration and production. Horizontally layered sedimentary rocks exhibit anisotropy that can be described by an effective transverse isotropic medium with a vertical axis of symmetry. Taking into account a vertically transverse isotropic earth, we derive phase-slowness expressions for quasi-P and quasi-SV waves which are used in a one-way wave-equation migration scheme. We derive simplified slowness-expressions which are useful for processing of conventional pressure data. Numerical examples demonstrate that the slowness approximations are valid for wide-angle propagation, and the resulting one-way propagators are validated on a series of synthetic tests and applied on a field ocean-bottom seismic dataset. The results show that the method accurately images both compressional and converted waves in OBS data over a vertically transverse isotropic medium.

INTRODUCTION

In seismic reflection surveying, by deploying both hydrophones and geophones at the seafloor as in e.g. ocean-bottom seismic (OBS) surveying, it is possible to record both pressure and shear-wave reflectors from the subsurface. By combining both pressure and shear-wave reflections, one can increase the amount of information about the subsurface than obtained with pressure waves alone (Hokstad, 2000). A dominant part of the seismic energy recorded on the horizontal geophone components is energy that has experienced conversion from pressure waves to shear waves at subsurface reflectors. Converted shear-wave data can possibly be used to image subsurface reflectors which are weak using pressure data alone, especially in gas-charged formations (Granli et al., 1999; MacLeod et al., 2005; Barkved et al., 2004), hence reducing the risk in hydrocarbon exploration and production. Shear-wave information may also help improve reservoir characterization by providing further constrains on rock properties, lithology, and fracture density and orientation.

The earth is anisotropic in nature and in particular sedimentary rocks exhibit anisotropy. These sedimentary rocks may often be described as being transverse isotropic with a symmetry axis perpendicular to the bedding plane. A homogeneous medium which is fractured may also be described as being transverse isotropic, now with a symmetry axis perpendicular to the fractures. A transversely isotropic media with a vertical symmetry axis (VTI) often presents a good model for the description of real rocks. The characteristics of wave-propagation in a VTI medium can be described by the dispersion relation, relating the vertical and horizontal phase-slowness. Seismic waves, and shear waves in particular, are sensitive to anisotropy.

There are several migration methods used in subsurface imaging. Depending on their underlying assumptions, these methods can usually be classified as either Kirchhoff (Schneider, 1978) or wavefield extrapolation (Bleistein, 1987; Gazdag, 1978; Stolt, 1978) methods. Kirchhoff methods explicitly introduce a high-frequency approximation of the wave-equation. In areas with complex geology where multi-pathing occures, Kirchhoff methods may not provide reliable subsurface images (Biondi, 2006). In wavefield extrapolation methods, multi-pathing is handled in a natural way. One-way wavefield extrapolation methods are routinely used in 3D depth migration of seismic data. Because of their efficient computer implementations and robustness, one-way methods have become increasingly popular and a wide variety of methods has been introduced (Gazdag, 1978; Stolt, 1978; Gazdag and

Sguazzero, 1984; Stoffa et al., 1990; Wu and Huang, 1992; Ristow and Rühl, 1994).

Utilizing an isotropic propagator for migration in a VTI medium may lead to position errors of subsurface structures (Larner and Cohen, 1993; Alkhalifah and Larner, 1994; Vestrum et al., 1999). In a VTI medium with no lateral variations where all medium parameters are known, the dispersion relation can be used directly in phase-shift (PS) migration methods (Gazdag, 1978), and provides an accurate description of the kinematics of wave-propagation. If we allow the medium to contain small lateral variations, a split-step Fourier (SSF) approach (Stoffa et al., 1990) account for the zero-order lateral perturbations in the medium parameters. To be able to exploit the phase-shift approach efficiently with a fast Fourier transform, and in addition provide an accurate description of wave-propagation in an isotropic laterally varying media, the scalar generalized-screen (Wu and Huang, 1992; Rousseau and de Hoop, 2001a) or Fourier finite-difference (FFD) method (Ristow and Rühl, 1994) can be used.

The isotropic FFD method was extended to VTI by Ristow and Rühl (1997) for quasi-P (qP) waves, and the isotropic generalized-screen approach was extended to VTI media by Rousseau and de Hoop (2001b). A simplified dispersion relation for qP waves was developed by Alkhalifah (1998, 2000). Based on this dispersion relation, Han and Wu (2005) develop a one-way propagator using a screen approximation with a finite difference correction term. Xie and Wu (2005) present a multicomponent prestack depth migration method utilizing the elastic screen method. Nolte (2005) describes a technique for converted-wave (C-wave) migration in anisotropic media with VTI symmetry using FFD methods through least-squares fitting of finite difference coefficients to an anisotropic dispersion relation.

We derive one-way propagators for compressional and converted-waves through a Fourier finite-difference approach based on a representation of the (squared) vertical slowness as a function of horizontal slowness. We provide a simplified vertical-slowness approximation involving fewer parameters which can be used in processing of compressional waves where not all medium parameters are available. The accuracy of the derived one-way propagators is demonstrated in 2D on synthetic data and in 3D on OBS field data from the Volve field in the central North sea.

THEORY

We consider a VTI medium which is described by its stiffness coefficients in the Voigt notation c_{ij}. For a VTI medium the only non-zero stiffness coefficients are (Thomsen, 1986)

$$\begin{bmatrix} c_{11} & c_{11}-2c_{66} & c_{13} & & & \\ c_{11}-2c_{66} & c_{11} & c_{13} & & & \\ c_{13} & c_{13} & c_{33} & & & \\ & & & c_{44} & & \\ & & & & c_{44} & \\ & & & & & c_{66} \end{bmatrix}. \quad (1)$$

In terms of density and stiffness coefficients, the vertical qP phase-velocity is given by

$$\alpha_0 = \sqrt{\frac{c_{33}}{\rho}}, \quad (2)$$

and the vertical quasi-SV (qSV) phase-velocity is given by

$$\beta_0 = \sqrt{\frac{c_{44}}{\rho}}, \quad (3)$$

where ρ denotes the density of the medium. The Thomsen (1986) parameters ε and δ are defined in terms of the stiffness coefficients by

$$\varepsilon = \frac{c_{11}-c_{33}}{2c_{33}}, \quad (4)$$

and

$$\delta = \frac{(c_{13}+c_{44})^2 - (c_{33}-c_{44})^2}{2c_{44}(c_{33}-c_{44})}, \quad (5)$$

and allows us to describe a VTI medium by the parameters α_0, β_0, δ and ε. For notational convenience, we introduce the parameters

$$\gamma_0 = \frac{\alpha_0}{\beta_0}, \quad (6)$$

$$\zeta = \varepsilon - \delta, \quad (7)$$

$$\sigma = \gamma_0^2 \zeta, \quad (8)$$

$$\eta = 1 + 2\delta. \quad (9)$$

The dispersion relation following from the stiffness coefficients in 1 via the Christoffel equation, relates the vertical and the horizontal slowness. This relation can be expressed in terms of the Thomsen parameters ε, δ and the vertical qP and the vertical qSV phase velocities α_0 and β_0. It can be solved for the squared vertical slowness q^2 as a function of horizontal-slowness p, both for qP- and qSV-wave modes.

From the dispersion relation, the squared vertical slowness for qP- and qSV-waves in a VTI medium can be expressed by (Stovas and Ursin, 2003; Ursin and Stovas, 2006)

$$\begin{aligned} q^2_{\alpha,\beta} =& \frac{1}{2}\left(q^2_{\alpha_0} + q^2_{\beta_0} - 2p^2(\sigma+\delta)\right) \\ & \mp \frac{1}{2}\left[\left(q^2_{\beta_0} - q^2_{\alpha_0}\right)^2 - 4\frac{p^2}{\alpha_0^2}\left(\gamma_0^2 - 1\right)(\sigma-\delta) \right. \\ & \left. + 4p^4\left(2\frac{(\gamma_0^2-1)}{\gamma_0^2}\sigma + (\sigma+\delta)^2\right)\right]^{\frac{1}{2}}, \end{aligned} \quad (10)$$

where $q^2_{\alpha_0} = 1/\alpha_0^2 - p^2$ and $q^2_{\beta_0} = 1/\beta_0^2 - p^2$. With no horizontal on-axis shear-wave triplication, the negative sign in front of the radical corresponds to the qP slowness and the positive sign corresponds to the qSV slowness. In case of a horizontal on-axis shear-wave triplication, q_β is multi-valued for some values of p (Pedersen et al., 2007). To get the vertical wave-number k_z, the vertical slowness q can be

written as $q = k_z/\omega$, while the horizontal-slowness p can be written $p = k_x/\omega$ where k_x is the lateral wave-number.

For simplicity in our derivations, we assume that we consider a 2D VTI medium where we can describe the parameters α_0 and β_0, and the anisotropy parameters ε and δ, as functions of both depth z and spatial position x. An extension to 3D is straight forward. To derive one-way propagators for migration, the medium is divided into thin depth-slabs of thickness Δz, where the parameters are assumed constant in depth within each slab and the lateral medium variations are smooth. Given a wavefield $\Psi(z,:)$ at some depth z, the solution of the one-way wave-equation provides the thin-slab propagator (Claerbout, 1985)

$$\Psi(z+\Delta z,:) = \mathrm{e}^{\pm \mathrm{i}\Delta z\omega q(p,x)}\Psi(z,:), \tag{11}$$

where the superscript sign corresponds to backward(-) and forward(+) propagation. Extrapolating the wavefield using equation 11 is expensive (Holberg, 1988). More efficient one-way propagators can be constructed by an approximation of the thin-slab propagator given in equation 11.

We will focus on an approximation of the thin-slab propagator similar to the FFD approach, as described by Ristow and Rühl (1994), where the propagator is separated into a PS propagator in a background medium and a spatial finite-difference correction accounting for the varying model components.

By introducing a constant background medium for each slab in a VTI medium, described by the parameters α_0^0, β_0^0, ε^0, and δ^0, we can represent the vertical slowness as

$$q_{\alpha,\beta}(p,x) = q^0_{\alpha,\beta}(p) + \Delta q_{\alpha,\beta}(p,x), \tag{12}$$

where $q^0_{\alpha,\beta}(p)$ denotes the vertical slowness in the background medium and $\Delta q_{\alpha,\beta}(p,x)$ denotes the phase-correcting term.

The wavefield is globally propagated in the background medium in vertical slowness domain using $q^0_{\alpha,\beta}(p)$, and locally corrected for the vertical-slowness perturbations with an approximation of the phase-correcting term $\Delta q_{\alpha,\beta}(p,x)$ through a finite-difference scheme in space. The vertical slowness is independent of lateral position in the background medium, hence we can accurately propagate the wavefield in the background medium utilizing a PS operator using the exact expression in equation 10.

When we consider the phase-correcting term, we notice that it is a non-linear function of both lateral position x and horizontal-slowness p, hence we need to decouple the spatial and horizontal-slowness dependency. Thus, for the phase-correcting term, we represent the vertical-slowness on the following form:

$$q_{\alpha,\beta} = \sum_{j\geq 0} k_j^{\alpha,\beta}(x)\, l_j^{\alpha,\beta}(p)\,. \tag{13}$$

By truncating the series expansion in equation 13, these expressions will provide a vertical-slowness approximation that can be used in constructing one-way propagators in an FFD approach after cascading by a continued-fraction approximation.

SLOWNESS EXPRESSIONS FOR QP- AND QSV-WAVES

By a series representation of the square-root term in equation 10, the squared qP slowness can be written as

$$q_\alpha^2 = \frac{1}{\alpha_0^2}\left(1 - \sum_{j\geq 0} a_j\,(p\alpha_0)^{2j+2}\right) \tag{14}$$

with

$$a_0 = 1 + 2\delta = \eta, \tag{15}$$

$$a_1 = \frac{2\sigma}{\gamma_0^2}\left(1 + \frac{2\gamma_0^2\delta}{\gamma_0^2 - 1}\right), \tag{16}$$

$$a_2 = \frac{-4\sigma}{\gamma_0^2\,(\gamma_0^2-1)}\,(\delta-\sigma)\left(1 + \frac{2\gamma_0^2\delta}{\gamma_0^2-1}\right). \tag{17}$$

The higher-order coefficients of the square-root expansion can be found in Ursin and Stovas (2006, equation B-9). To express the vertical slowness for qP-waves on polynomial form as given in equation 13 (and hence being able to separate the spatial and wave-number dependencies), we take the square-root of equation 14.

By a Taylor expansion of the square root of equation 14 around $p = 0$ we obtain

$$q_\alpha = \frac{1}{\alpha_0}\left(1 - \sum_{j\geq 0} \tilde{a}_j\,(p\alpha_0)^{2j+2}\right) \tag{18}$$

where the first coefficients $\tilde{a}_j$ in terms of a_j are

$$\tilde{a}_0 = \frac{1}{2}a_0, \tag{19}$$

$$\tilde{a}_1 = \frac{1}{2}a_1 + \frac{1}{8}a_0^2, \tag{20}$$

$$\tilde{a}_2 = \frac{1}{2}a_2 + \frac{1}{4}a_0a_1 + \frac{1}{16}a_0^3, \tag{21}$$

thus q_α is on desired form as represented in equation 13.

For qSV-waves, we find a series expansion of the squared vertical slowness as:

$$q_\beta^2 = \frac{1}{\beta_0^2}\left(1 - \sum_{j\geq 0} c_j\,(p\beta_0)^{2j+2}\right) \tag{22}$$

where

$$c_0 = 1 + 2\sigma, \tag{23}$$

$$c_j = -a_j\gamma_0^{2j}, \qquad j \geq 1. \tag{24}$$

By a similar approach as for the slowness approximation of qP-waves, we find a slowness approximation for qSV-waves given by

$$q_\beta = \frac{1}{\beta_0}\left(1 - \sum_{j\geq 0} \tilde{c}_j\,(p\beta_0)^{2j+2}\right) \tag{25}$$

where the first coefficients $\tilde{c}_j$ in terms of c_j are

$$\tilde{c}_0 = \frac{1}{2}c_0, \tag{26}$$

$$\tilde{c}_1 = \frac{1}{2}c_1 + \frac{1}{8}c_0^2, \tag{27}$$

$$\tilde{c}_2 = \frac{1}{2}c_2 + \frac{1}{4}c_0c_1 + \frac{1}{16}c_0^3. \tag{28}$$

The representation of the qP- and qSV-slowness can now be cascaded by continued-fraction approximations. By cascading the expression in 18, we find that the qP slowness can be approximated by

$$q_\alpha = \frac{1}{\alpha_0}\left(1 + \kappa_2^\alpha p^2 + \frac{\kappa_1^\alpha p^2}{1 - \kappa_0^\alpha p^2}\right), \tag{29}$$

where

$$\kappa_0^\alpha = \frac{\tilde{a}_2}{\tilde{a}_1}\alpha_0, \tag{30}$$

$$\kappa_1^\alpha = \frac{\tilde{a}_1^2}{\tilde{a}_2}\alpha_0^2, \tag{31}$$

$$\kappa_2^\alpha = \left(\tilde{a}_0 - \frac{\tilde{a}_1^2}{\tilde{a}_2}\right)\alpha_0. \tag{32}$$

Similar for the qSV-waves, by cascading the slowness approximation for qSV-waves in equation 25, we find

$$q_\beta = \frac{1}{\beta_0}\left(1 + \kappa_2^\beta p^2 + \frac{\kappa_1^\beta p^2}{1 - \kappa_0^\beta p^2}\right), \tag{33}$$

where

$$\kappa_0^\beta = \frac{\tilde{c}_2}{\tilde{c}_1}\beta_0, \tag{34}$$

$$\kappa_1^\beta = \frac{\tilde{c}_1^2}{\tilde{c}_2}\beta_0^2, \tag{35}$$

$$\kappa_2^\beta = \left(\tilde{c}_0 - \frac{\tilde{c}_1^2}{\tilde{c}_2}\right)\beta_0. \tag{36}$$

SIMPLIFIED SLOWNESS EXPRESSIONS FOR QP-WAVES

For conventional towed streamer data, only qP-waves are recorded. In this case it is convenient to consider simplified expressions of the vertical slowness for qP-waves where the qSV-wave velocity is disregarded, i.e. a quasi-acoustic approximation (Alkhalifah, 1998). In the quasi-acoustic approximation, we assume that $\gamma_0^2 \gg 1$, and a simplified slowness expression for qP waves can be provided by (Alkhalifah, 1998; Pedersen et al., 2007)

$$q_\alpha^s = \frac{1}{\alpha_0}\sqrt{\frac{1 - (1+2\varepsilon)(p\alpha_0)^2}{1 - 2\zeta(p\alpha_0)^2}}, \tag{37}$$

where the superscript s denotes a quasi-acoustic approximation.

From the quasi-acoustic approximation and equations 15 through 17, we find

$$a_0^s = \eta, \tag{38}$$

$$a_1^s = 2\eta\zeta, \tag{39}$$

$$a_2^s = 4\zeta^2\eta, \tag{40}$$

Parameters	α_0 km/s	β_0 km/s	ε	δ
Model 1	2.0	1.0	0.10	0.05
Model 2	2.0	1.0	0.10	0.15

Table 1: Model parameters used for computing slowness approximations.

and the Taylor-expanded vertical-slowness can be approximated by the truncated series

$$q_\alpha^s = \frac{1}{\alpha_0}\left(1 - \sum_{j=0}^{2} a_j^s (p\alpha_0)^{2j+2}\right). \tag{41}$$

By substituting the simplified parameters a_j^s into equations 30 through 32 we find

$$\kappa_0^{\alpha,s} = \frac{2\zeta^2 + \frac{1}{2}\zeta\eta + \frac{1}{16}\eta^2}{\zeta + \frac{1}{8}\eta}\alpha_0, \tag{42}$$

$$\kappa_1^{\alpha,s} = \frac{\zeta^2\eta^2 + \frac{1}{4}\zeta\eta^3 + \frac{1}{64}}{2\zeta^2\eta + \frac{1}{2}\zeta\eta^2 + \frac{1}{16}\eta^3}\alpha_0^2, \tag{43}$$

$$\kappa_2^{\alpha,s} = \left(\frac{1}{2}\eta - \frac{\zeta^2\eta^2 + \frac{1}{4}\zeta\eta^3 + \frac{1}{64}}{2\zeta^2\eta + \frac{1}{2}\zeta\eta^2 + \frac{1}{16}\eta^3}\right)\alpha_0. \tag{44}$$

Thus, a simplified cascaded qP-slowness expression can be found by inserting the simplified coefficients $\kappa_i^{\alpha,s}$ into equation 29, that is

$$q_\alpha^s = \frac{1}{\alpha_0}\left(1 + \kappa_2^{\alpha,s} p^2 + \frac{\kappa_1^{\alpha,s} p^2}{1 - \kappa_0^{\alpha,s} p^2}\right). \tag{45}$$

ACCURACY OF SLOWNESS EXPRESSIONS

We compare the accuracy of the Taylor-expanded slowness expressions in equations 18 and 25 and the cascaded slowness expressions in equations 29 and 33 for qP and qSV waves, respectively. The performance of the slowness approximations is illustrated using two models as given in table 1, where the Taylor-expanded series are truncated at $j = 2$. We also show the accuracy of the quasi-acoustic qP slowness expression as given in equation 41 on polynomial form and equation 45 on cascaded form.

The medium parameters in model 1 is defined by $\alpha_0 = 2.00$ km/s, $\beta_0 = 1.00$ km/s, $\varepsilon = 0.10$ and $\delta = 0.05$ and the medium parameters in model 2 is defined by $\alpha_0 = 2.00$ km/s, $\beta_0 = 1.00$ km/s, $\varepsilon = 0.10$ and $\delta = 0.10$. In figures 1(a) and 1(b) we plot the derived slowness curves for qP- and qSV-waves in model 1, respectively. We see that for small angles, the qP and qSV Taylor-expanded slowness curves are accurate. The accuracy of the cascaded approximations are comparable to that of the Taylor-expanded slowness curve. For intermediate and wide angles, the cascaded approximation performs better. Similar results are found for model 2, as illustrated in figures 2(a) and 2(b).

The derived quasi-acoustic slowness curves for model 1 and 2 are shown in figures 3(a) and 3(b). As for the qP-waves, the accuracy of the quasi-acoustic cascaded approximation is better for intermediate and larger angles

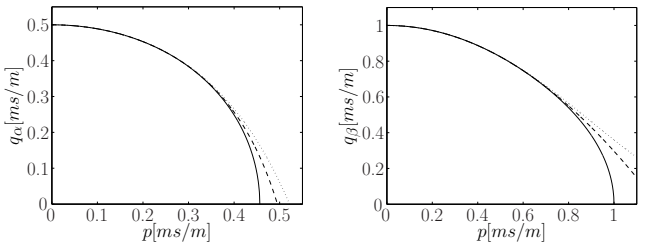

(a) (b)

Figure 1: Slowness surfaces for $\alpha_0 = 2.0$ km/s, $\beta_0 = 1.0$ km/s, $\varepsilon = 0.10$ and $\delta = 0.05$. (a) The exact qP slowness curve in solid line; the Taylor-expanded qP slowness curve in dotted line; and the cascaded qP slowness curve in dashed line. (b) The exact qSV slowness curve in solid line; the Taylor-expanded qSV slowness curve in dotted line; and the cascaded qSV slowness curve in dashed line.

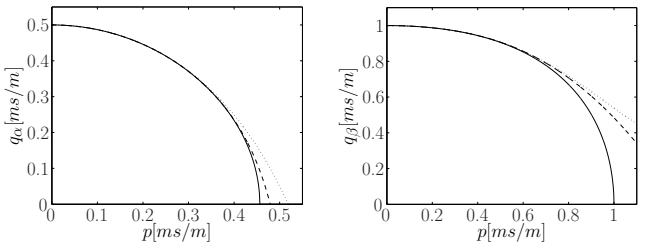

(a) (b)

Figure 2: Slowness surfaces for $\alpha_0 = 2.0$ km/s, $\beta_0 = 1.0$ km/s, $\varepsilon = 0.10$ and $\delta = 0.15$. (a) The exact qP slowness curve in solid line; the Taylor-expanded qP slowness curve in dotted line; and the cascaded qP slowness curve in dashed line. (b) The exact qSV slowness curve in solid line; the Taylor-expanded qSV slowness curve in dotted line; and the cascaded qSV slowness curve in dashed line.

than the quasi-acoustic Taylor-expanded slowness curves.

ONE-WAY PROPAGATORS

Introducing a laterally invariant background medium allows us to define a vertical slowness perturbation Δq_α using equation 18. Further, by cascading Δq_α as given in equation 29, from equation 11 the resulting one-way propagator for qP-waves can be represented by

$$\mathrm{e}^{\mathrm{i}\omega\Delta z q_\alpha(p,x)} \approx \mathrm{e}^{\mathrm{i}\omega\Delta z q^0_\alpha(p)}\mathrm{e}^{\mathrm{i}\omega\Delta z\Delta q_\alpha(p,x)}. \qquad (46)$$

See the Appendix for a detailed derivation. In a similar fashion, we find that the qSV propagator can be represented by

$$\mathrm{e}^{\mathrm{i}\omega\Delta z q_\beta(p,x)} \approx \mathrm{e}^{\mathrm{i}\omega\Delta z q^0_\beta(p)}\mathrm{e}^{\mathrm{i}\omega\Delta z\Delta q_\beta(p,x)}. \qquad (47)$$

For the quasi-acoustic case, we can represent the qP propagator as

$$\mathrm{e}^{\mathrm{i}\omega\Delta z q_\alpha(p,x)} \approx \mathrm{e}^{\mathrm{i}\omega\Delta z q^{s,0}_\alpha(p)}\mathrm{e}^{\mathrm{i}\omega\Delta z\Delta q^s_\alpha(p,x)}, \qquad (48)$$

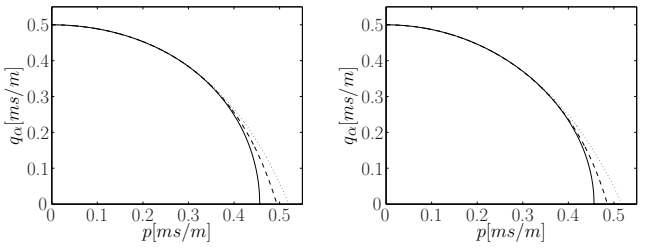

(a) (b)

Figure 3: (a) Slowness surfaces for $\alpha_0 = 2.0$ km/s, $\beta_0 = 1.0$ km/s, $\varepsilon = 0.10$ and $\delta = 0.05$. (b) Slowness surfaces for $\alpha_0 = 2.0$ km/s, $\beta_0 = 1.0$ km/s, $\varepsilon = 0.10$ and $\delta = 0.15$. The exact qP slowness curve in solid line; the quasi-acoustic Taylor-expanded qP slowness curve in dotted line; and the quasi-acoustic cascaded qP slowness curve in dashed line.

where $q^{s,0}_\alpha$ is given by the simplified dispersion relation in equation 37 and Δq^s_α is found by cascading the vertical slowness perturbation as given in equation 45.

For each frequency, the PS in the background medium is applied to the wavefield in slowness domain, while the phase-correcting term handling the vertical-slowness perturbation is applied in space domain by a finite-difference approach in a similar fashion as described by Ristow and Rühl (1994).

In an OBS experiment with a downgoing pressure source field (D^{qP}) in a fluid and by recording pressure and particle velocity at the seafoor, we can find the upgoing pressure wavefield (U^{qP}) and the upgoing shear wavefield (U^{qSV}) at the sea floor by wavefield decomposition (Amundsen and Reitan, 1995; Osen et al., 1996).

A C-wave subsurface image, denoted $I^{qP,qSV}$, can found by

$$I^{qP,qSV}(z,:) = \sum_k \sum_\omega U^{qSV}_k(z,:) D^{qP}_k(z,:)^* \qquad (49)$$

and a $qP - qP$ subsurface image, denoted $I^{qP,qP}$, can found by

$$I^{qP,qP}(z,:) = \sum_k \sum_\omega U^{qP}_k(z,:) D^{qP}_k(z,:)^*, \qquad (50)$$

where the superscript $*$ denotes complex conjugate (Claerbout, 1971) and

$$D^{qP}(z+\Delta z,:) = \mathrm{e}^{\mathrm{i}\omega\Delta z q_\alpha(p,x)} D^{qP}(z,:) \qquad (51)$$
$$U^{qP}(z+\Delta z,:) = \mathrm{e}^{-\mathrm{i}\omega\Delta z q_\alpha(p,x)} U^{qP}(z,:) \qquad (52)$$
$$U^{qSV}(z+\Delta z,:) = \mathrm{e}^{-\mathrm{i}\omega\Delta z q_\beta(p,x)} U^{qSV}(z,:). \qquad (53)$$

The subscript k denotes shot number for common-shot migration and receiver number for common-receiver migration.

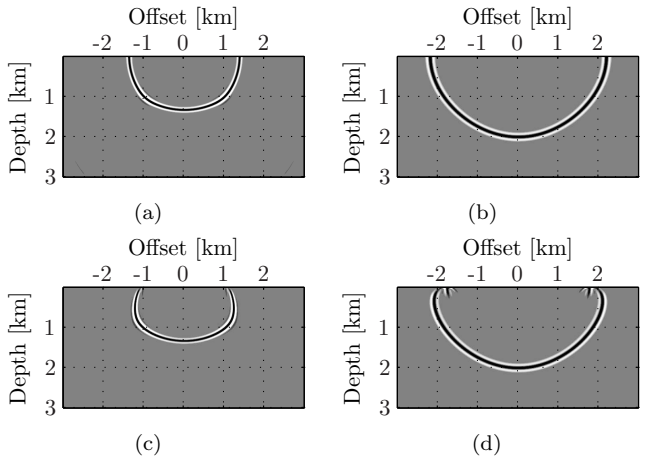

Figure 4: Impulse responses of $qP - qSV$ (left) and $qP - qP$ (right) waves without medium perturbation (top) and with medium perturbations (bottom).

NUMERICAL RESULTS

Impulse responses

To demonstrate the accuracy of the derived one-way propagators, we first produce a series of impulse response tests. The impulse response test involves migrating a single input seismic trace in a given medium. The input trace contains a single spike located at time 2.0 s.

We consider a medium given by $\alpha_0 = 2000.0$ m/s, $\beta_0 = 1000.0$ m/s, $\delta = 0.0$ and $\varepsilon = 0.1$. By introducing a background medium given by $\alpha_0^0 = 1500.0$ m/s, $\beta_0^0 = 750.0$ m/s, $\delta^0 = 0.0$ and $\varepsilon^0 = 0.1$ we can illustrate the ability of the derived one-way propagators to handle the resulting lateral medium variations.

The impulse response resulting from the C-wave migration without perturbations is shown in figure 4(a). Without medium perturbations, the propagators used in the C-wave migration reduce to PS since the phase-correcting term in the resulting one-way propagators become unity. Since we have propagated in a medium with constant model parameters, the PS provides an accurate positioning of the impulse response. The resulting impulse response for the C-wave migration including the perturbations is shown in figure 4(c). We see that the proposed one-way propagators in this example are accurate for small and intermediate angles. For larger angles the error introduced by the medium perturbations cause the impulse response to be mis-positioned. This is mainly due to the inaccuracy of the qSV slowness approximation for large angles, which diverges from the exact qSV slowness.

In figure 4(b), the $qP - qP$ impulse response without perturbations is shown. As for the C-wave migration, we can assume that the $qP - qP$ PS propagator provides an accurate positioning of the wavefronts. The corresponding impulse response with perturbations is shown in figure 4(d). The $qP - qP$ migration with a phase-correcting term handling the perturbations provide an accurate result.

The impulse responses from the simplified quasi-acoustic one-way propagator are shown in figure 5, where the impulse response in the constant background medium is shown in figure 5(a) and the impulse response in the medium containing perturbations is shown in figure 5(b). As for the $qP - qP$ propagator, we see that the proposed quasi-acoustic propagator position the wavefront accurately.

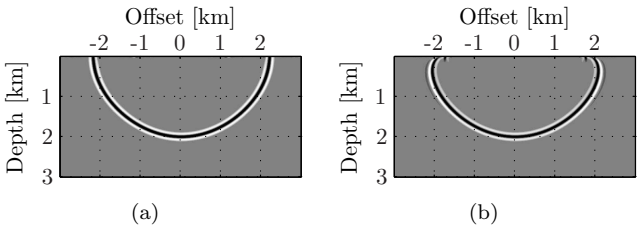

Figure 5: Impulse responses of the quasi-acoustic $qP - qP$ waves (a) without medium perturbation and (b) with medium perturbations.

In general, the accuracy of the derived one-way propagators for high dips depends on the variation of the medium properties. That is, for high dips the propagators are more accurate for small medium variations than for larger medium variations.

2D Synthetic data example

Next, the accuracy of the kinematics of the proposed one-way propagators is demonstrated on a 2D synthetic dataset.

A synthetic common-shot dataset was produced using a Born-Kirchhoff-Helmholtz modelling scheme (Ursin and Tygel, 1997; Sollid and Ursin, 2003) both for $qP-qP$ and $qP-qSV$ waves. The dataset model parameters are shown in figure 6. The model consists of 5 reflecting interfaces and the response from the sea-floor is not modelled. The sources are located at the sea surface, while the receiver cable is located at the seafloor at depth 100 m. Each shot contains 161 receivers with separated by 20 m, and the shots are distributed with a distance of 20 m. Figure 7 depict selected shot-gathers which are input to migration.

The migrated sections are shown in figure 8, where figure 8(a) depicts the migrated $qP - qP$ data and figure 8(b) depicts the migrated $qP - qSV$ data. Above the sea-floor, $\beta_0 = \delta = \varepsilon = 0$, thus the downgoing source pressure wavefield U^{qP} is propagated using an isotropic phase-shift down to the sea-floor. From the results, we see that both the C-wave and $qP - qP$-wave migration provide accurate results. The difference between the migrated sections is not very distinct, and the reflector interpretation would most likely coincide for both sections.

The migrated section resulting from the simplified quasi-acoustic propagator is shown in figure 9. We see that the results are comparable to the $qP - qP$ migration.

3D Real ocean-bottom data example

Finally, the derived one-way propagators are applied to a 3D field OBS dataset. The OBS data in our field data example was acquired in 2002 in the central North Sea

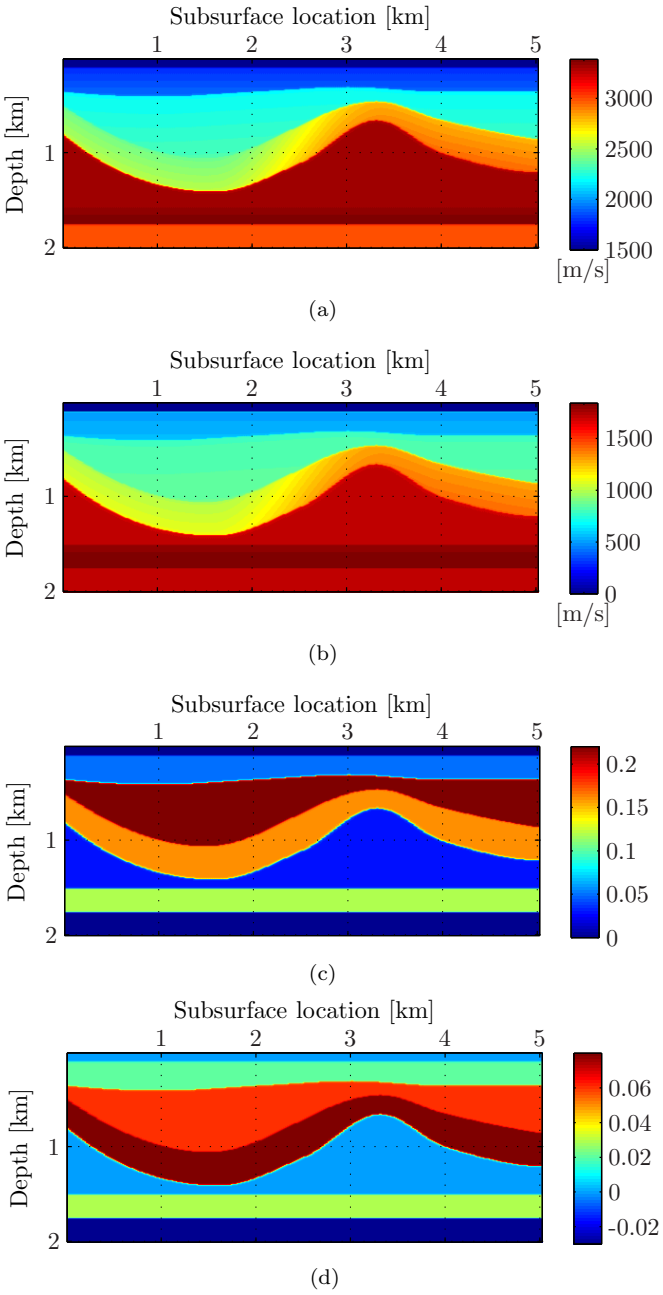

Figure 6: Model parameters for the synthetic data example. (a) Vertical qP-wave velocity α_0; (b) vertical qSV-wave velocity β_0; (c) Thomsen parameter δ; and (e) Thomsen parameter ε.

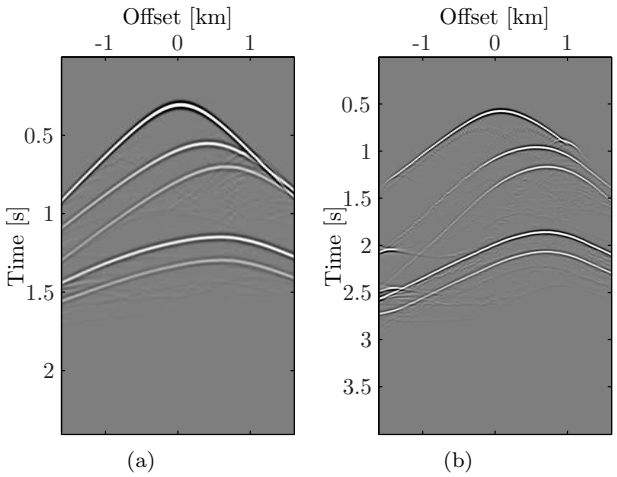

Figure 7: Selected synthetic shot-gathers - for a source at surface location 2500 m - which are input to migration. (a) $qP-qP$ shot gather and (b) $qP-qSV$ shot gather.

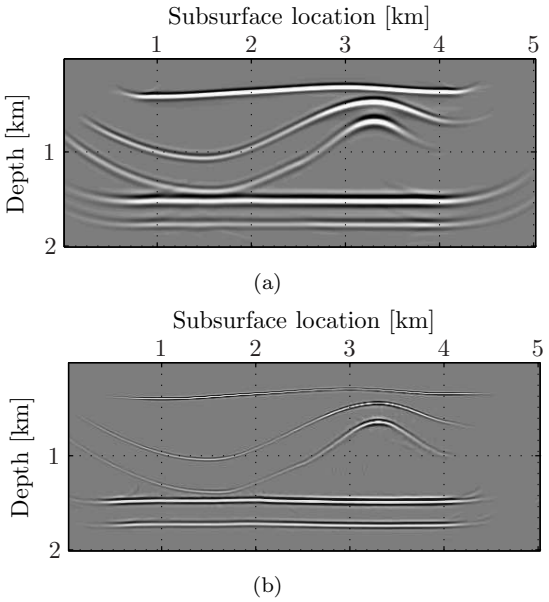

Figure 8: Migrated section of the synthetic data example. (a) $qP-qP$-stack and (b) $qP-qSV$-stack.

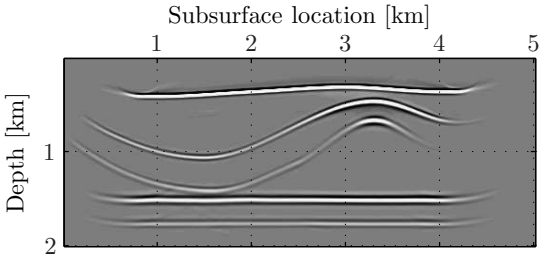

Figure 9: Migrated section of the synthetic data example. Quasi-acoustic $qP-qP$-stack.

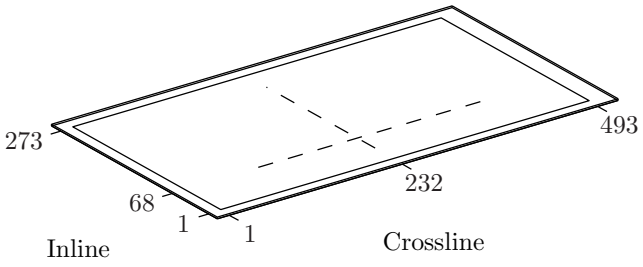

Figure 10: Representation of the geometry used in migration of the 3D field data example. Extracted I^{qP-qP} and I^{qP-qSV} sections are indicated by dashed lines and displayed if figures 13; 14; 15; and 16.

over the Volve field. The field is located in the Sleipner area in the southern part of the Viking Graben.

A subset of the entire 3D survey was extracted for input to a common-receiver migration scheme. A 2D section of the derived model parameters (Szydlik et al., 2007) are shown in figure 11, where figure 11(a) shows the vertical qP-wave velocity; figure 11(b) shows the vertical qSV-wave velocity; figure 11(c) shows the Thomsen parameter δ; and figure 11(d) shows the Thomsen parameter ε. The extracted dataset contains 12 cables of 6 km length, each with 240 receivers. The shots are separated by 50-by-50 m. In figure 12, selected shot-gathers which are sorted into common-receiver gathers and input to migration are shown, where figure 12(a) shows a $qP-qP$ gather and figure 12(b) shows a $qP-qSV$ gather.

From the stacked migrated datasets I^{qP-qP} and I^{qP-qSV} we extract two sections; one along (inline 68) and one across (crossline 232) the OBS cables indicated by the dashed lines in figure 10. The sections I^{qP-qP} and I^{qP-qSV} for inline 68 are shown in figure 13 and 14, respectively. The sections I^{qP-qP} and I^{qP-qSV} for crossline 232 are shown in figure 15 and 16, respectively. No post-processing has been applied after imaging except a gain in depth for displaying purposes.

In general, the migrated images I^{qP-qP} and I^{qP-qSV} show good structural focusing. The two images correlate well in depth. We notice that the migrated I^{qP-qP} image show better reflector continuity in the deeper part than the migrated I^{qP-qSV} image and thereby seems to be better focused. Some differences are found between the distinction of some of the reflectors. These differences are most probably due to differences in the reflectivity for the converted waves. Another issue worth mentioning is that the converted images are potentially more sensitive to errors in the anisotropy parameters.

CONCLUSION

We have derived accurate representations of the qP and qSV slowness in a VTI medium which provide accurate one-way propagators. In the appendix, we have shown that in the isotropic case, the derived propagators reduce to the third-order Fourier finite-difference propagators de-

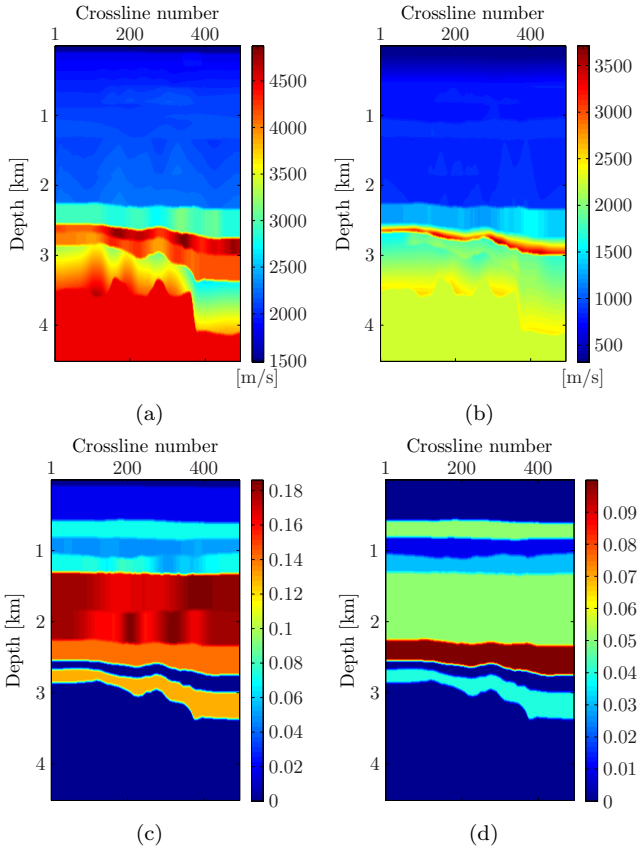

Figure 11: Model parameters for the real data example from offshore Norway at inline 68. (a) Vertical qP-wave velocity α_0; (b) vertical qSV-wave velocity β_0; (c) Thomsen parameter δ; and (e) Thomsen parameter ε.

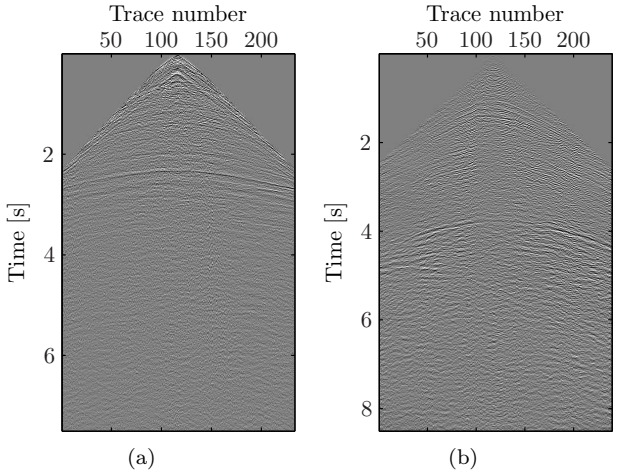

Figure 12: Selected shot gathers which are sorted into common-receiver gathers and input to migration for the real data example from offshore Norway. (a) Derived $qP-qP$ shot-gathers and (b) derived $qP-qSV$ shot-gather.

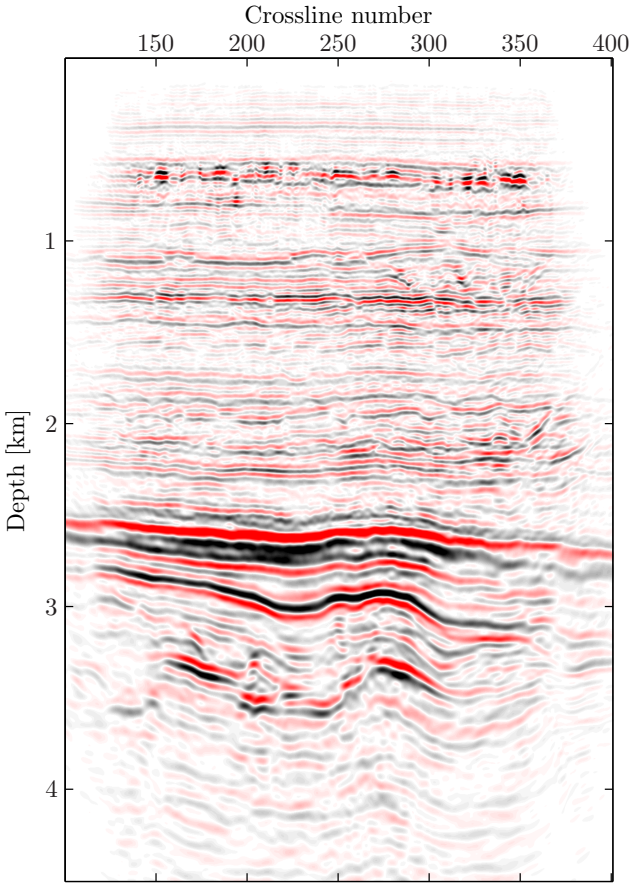

Figure 13: Migrated $qP-qP$ section from inline 68 of the real data example from offshore Norway.

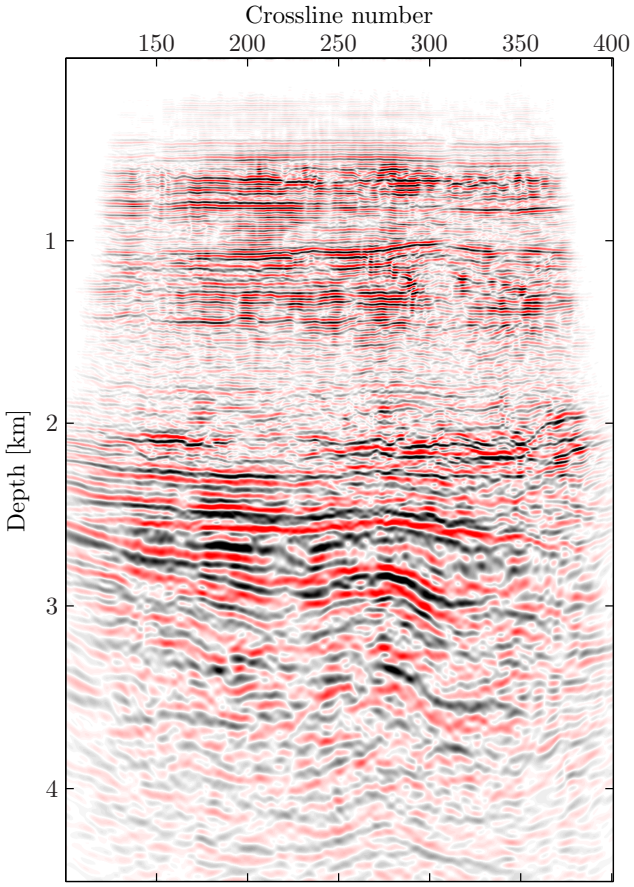

Figure 14: Migrated $qP-qSV$ section from inline 68 of the real data example from offshore Norway.

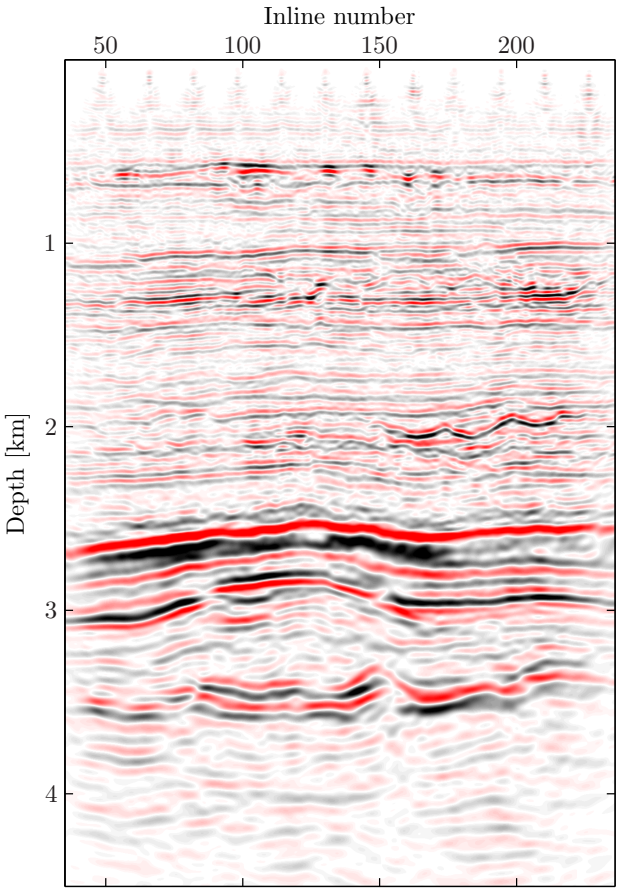

Figure 15: Migrated $qP - qP$ section from crossline 232 of the real data example from offshore Norway.

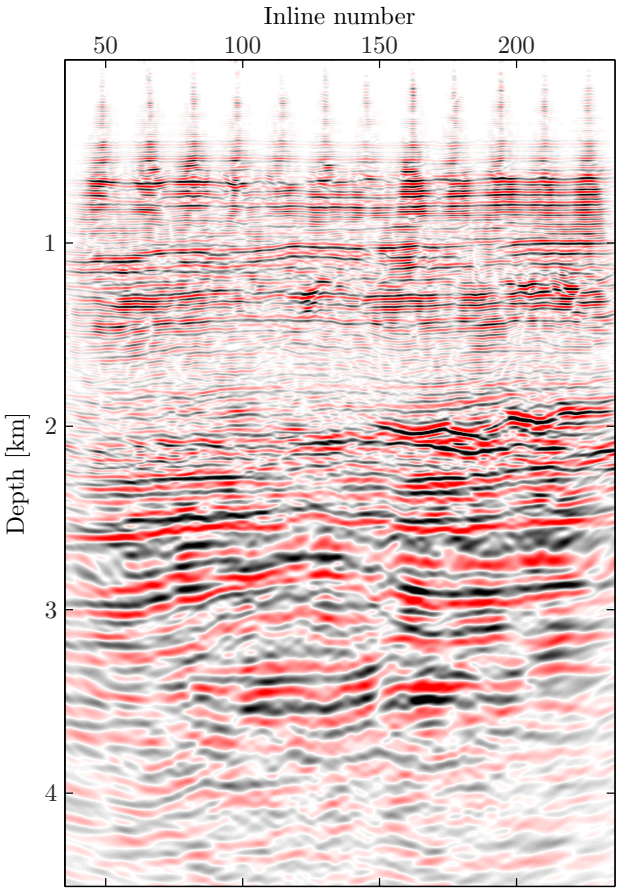

Figure 16: Migrated $qP - qSV$ section from crossline 232 of the real data example from offshore Norway.

scribed by Ristow and Rühl (1994). We have derived simplified expressions useful for conventional processing of compressional waves in a VTI medium where the qSV-wave velocity is unknown. The derived one-way propagators are tested on a series of synthetic tests and applied on a field OBS dataset The results show that the proposed propagators can be used for accurate imaging of field OBS data over a VTI medium for both compressional and C-waves.

ACKNOWLEDGMENT

This research was supported by the Norwegian Research Council via the ROSE project. We would like to thank Statoil ASA for permission to publish and providing the field dataset. ØP would like to thank Joachim Mispel for help preparing the field data. Bjørn Ursin has received financial support from Statoil ASA through the VISTA project.

APPENDIX A

FINITE-DIFFERENCE CORRECTIONS FOR ONE-WAY THIN-SLAB PROPAGATORS

Using equation 18, we find that we can represent the phase-correcting term Δq_α as

$$\begin{aligned}\Delta q_\alpha &= q_\alpha - q_\alpha^0 \\ &= \frac{1}{\alpha_0}(1-r) - \sum_{j\geq 0}\left(\tilde{a}_j - \tilde{a}_j^0 r^{2j+2}\right)(\alpha_0 p)^{2j+2}\end{aligned} \tag{A-1}$$

where $r = \alpha_0^0/\alpha_0$ and $\tilde{a}_j^0$ are the coefficients in equations 19 through 21 defined by the background medium. By cascading Δq_α as given in equation 29, we find that

$$\Delta q_\alpha \approx \frac{1}{\alpha_0}(1-r) + \Delta\kappa_2^\alpha p^2 + \frac{\Delta\kappa_1^\alpha p^2}{1-\Delta\kappa_0^\alpha p^2}, \tag{A-2}$$

where

$$\begin{aligned}\Delta\kappa_0^\alpha &= \frac{\Delta s_1^2}{\Delta s_2}\alpha_0 \\ \Delta\kappa_1^\alpha &= \frac{\Delta s_2}{\Delta s_1}\alpha_0 \\ \Delta\kappa_2^\alpha &= \left(\Delta s_0 - \frac{\Delta s_1^2}{\Delta s_2}\right)\alpha_0\end{aligned} \tag{A-3}$$

and

$$\begin{aligned}\Delta s_0 &= \tilde{a}_0 - \tilde{a}_0^0 r \\ \Delta s_1 &= \tilde{a}_1 - \tilde{a}_1^0 r^3 \\ \Delta s_2 &= \tilde{a}_2 - \tilde{a}_2^0 r^5.\end{aligned} \tag{A-4}$$

Similarly, from equation 29 we find

$$\begin{aligned}\Delta q_\beta &= q_\beta - q_\beta^0 \\ &= \frac{1}{\beta_0}(1-t) - \sum_{j\geq 0}\left(\tilde{c}_j - \tilde{c}_j^0 t^{2j+2}\right)(\beta_0 p)^{2j+2}\end{aligned} \tag{A-5}$$

where $t = \beta_0^0/\beta_0$ and $\tilde{c}_j^0$ are the coefficients in equations 26 through 28 defined by the background medium. By cascading Δq_β as given in equation 33, we find that

$$\Delta q_\beta \approx \frac{1}{\beta_0}(1-t) + \Delta\kappa_2^\beta p^2 + \frac{\Delta\kappa_1^\beta p^2}{1-\Delta\kappa_0^\beta p^2}, \tag{A-6}$$

where

$$\begin{aligned}\Delta\kappa_0^\beta &= \frac{\Delta u_1^2}{\Delta u_2}\beta_0 \\ \Delta\kappa_1^\beta &= \frac{\Delta u_2}{\Delta u_1}\beta_0^2 \\ \Delta\kappa_2^\beta &= \left(\Delta u_0 - \frac{\Delta u_1^2}{\Delta u_2}\right)\beta_0\end{aligned} \tag{A-7}$$

and

$$\begin{aligned}\Delta u_0 &= \tilde{u}_0 - \tilde{u}_0^0 t \\ \Delta u_1 &= \tilde{u}_1 - \tilde{u}_1^0 t^3 \\ \Delta u_2 &= \tilde{u}_2 - \tilde{u}_2^0 t^5.\end{aligned} \tag{A-8}$$

Finally, we notice that in the isotropic case, $\zeta = \sigma = 0$ and $\eta = 1$, thus $a_0 = 1$ and $a_1 = a_2 = 0$, hence,

$$\begin{aligned}\tilde{a}_0 &= \frac{1}{2}, \\ \tilde{a}_1 &= \frac{1}{8}, \\ \tilde{a}_2 &= \frac{1}{16}.\end{aligned} \tag{A-9}$$

This gives

$$\begin{aligned}\Delta s_0 &= \frac{1}{2}(1-r), \\ \Delta s_1 &= \frac{1}{8}(1-r^3), \\ \Delta s_2 &= \frac{1}{16}(1-r^5).\end{aligned} \tag{A-10}$$

Further,

$$\begin{aligned}\Delta\kappa_0^\alpha &= \frac{1}{4}\frac{(1-r^3)^2}{1-r^5}\alpha_0, \\ \Delta\kappa_1^\alpha &= \frac{1}{2}\frac{1-r^5}{1-r^3}\alpha_0^2, \\ \Delta\kappa_2^\alpha &= \left(\frac{1}{2}(1-r) - \frac{1}{4}\frac{(1-r^3)^2}{1-r^5}\right)\alpha_0,\end{aligned} \tag{A-11}$$

which is equivalent to the isotropic third-order FFD approximation derived by Ristow and Rühl (1994, their equation A-22).

REFERENCES

Alkhalifah, T., 1998, Acoustic approximations for processing in transversely isotropic media: Geophysics, **63**, 623–631.

———, 2000, An acoustic wave equation for anisotropic media: Geophysics, **65**, 1239–1250.

Alkhalifah, T. and K. Larner, 1994, Migration error in transversely isotropic media: Geophysics, **59**, 1405–1418.

Amundsen, L. and A. Reitan, 1995, Decomposition of multicomponent sea-floor data into upgoing and downgoing P- and S-waves: Geophysics, **60**, 563–572.

Barkved, O., B. Bartman, B. Compani, J. Gaiser, R. VanDok, T. Johns, P. Kristiansen, T. Probert, and M. Thompson, 2004, The many facets of multicomponent seismic data: Oilfield Review, Summer, 42–56.

Biondi, B., 2006, 3D Seismic Imaging: Vol. 14, Investigations in Geophysics Series,SEG, Tulsa, OK.

Bleistein, N., 1987, On the imaging of reflectors in the earth: Geophysics, **52**, 931–942.

Claerbout, J. F., 1971, Toward a unified theory of reflector mapping: Geophysics, **36**, 467–481.

———, 1985, Imaging the earth's interior: Blackwell Scientific Publications.

Gazdag, J., 1978, Wave equation migration with the phase-shift method: Geophysics, **43**, 1342–1351.

Gazdag, J. and P. Sguazzero, 1984, Migration of seismic data by phase shift plus interpolation: Geophysics, **49**, 124–131.

Granli, J., B. Arntsen, A. Sollid, and E. Hilde, 1999, Imaging through gas-filled sediments using marine shear-wave data: Geophysics, **64**, 668.

Han, Q. and R.-S. Wu, 2005, A one-way dual-domain propagator for scalar qP-waves in VTI media: Geophysics, **70**, D9–D17.

Hokstad, K., 2000, Multicomponent Kirchhoff migration: Geophysics, **65**, 861.

Holberg, O., 1988, Towards optimum one-way wave propagation: Geophysical Prospecting, **36**, 99–114.

Larner, K. L. and J. K. Cohen, 1993, Migration error in transversely isotropic media with linear velocity variation in depth: Geophysics, **58**, 1454–1467.

MacLeod, M., R. Hanson, M. Hadley, K. Reynolds, D. Lumley, S. McHugo, and T. Probert, 2005, The Alba field OBC seismic survey: 61 st Ann. Mtg., Eur. Assn. Geosci. Eng.

Nolte, B., 2005, Converted-wave migration for VTI media using Fourier finite-difference depth extrapolation: 67th Annual Internat. Mtg., EAGE, Expanded Abstracts, P001.

Osen, A., L. Storelvmo, L. Amundsen, and A. Reitan, 1996, Decomposition of particle velocity fields into up- and downgoing P- and S-waves: SEG Technical Program Expanded Abstracts, **15**, 743–746.

Pedersen, Ø., B. Ursin, and A. Stovas, 2007, Wide-angle phase-slowness approximations in VTI media: Geophysics, **72**, S177–S185.

Ristow, D. and T. Rühl, 1994, Fourier finite-difference migration: Geophysics, **59**, 1882.

———, 1997, Migration in transversely isotropic media using implicit operators: SEG Technical Program Expanded Abstracts, **16**, 1699–1702.

Rousseau, J. H. L. and M. V. de Hoop, 2001a, Modeling and imaging with the scalar generalized-screen algorithms in isotropic media: Geophysics, **66**, 1551–1568.

———, 2001b, Scalar generalized-screen algorithms in transversely isotropic media with a vertical symmetry axis: Geophysics, **66**, 1538–1550.

Schneider, W., 1978, Integral formulation for migration in two and three dimensions: Geophysics, **43**, 49.

Sollid, A. and B. Ursin, 2003, Scattering-angle migration of ocean-bottom seismic data in weakly anisotropic media: Geophysics, **68**, 641–655.

Stoffa, P. L., J. T. Fokkema, R. M. de Luna Freire, and W. P. Kessinger, 1990, Split-step Fourier migration: Geophysics, **55**, 410–421.

Stolt, R. H., 1978, Migration by Fourier transform: Geophysics, **43**, 23–48.

Stovas, A. and B. Ursin, 2003, Reflection and transmission responses of layered transversely isotropic viscoelastic media: Geophysical Prospecting, **51**, 447–477.

Szydlik, T., P. Smith, S. Way, L. Aamodt, and C. Friedrich, 2007, 3D PP/PS prestack depth migration on the Volve field: First Break, 43.

Thomsen, L., 1986, Weak elastic anisotropy: Geophysics, **51**, 1954–1966.

Ursin, B. and A. Stovas, 2006, Traveltime approximations for a layered transversely isotropic medium: Geophysics, **71**, D23–D33.

Ursin, B. and M. Tygel, 1997, Reciprocal volume and surface scattering integrals for anisotropic elastic media: Wave Motion, **26**, 31–42.

Vestrum, R. W., D. C. Lawton, and R. Schmid, 1999, Imaging structures below dipping TI media: Geophysics, **64**, 1239–1246.

Wu, R.-S. and L.-J. Huang, 1992, Scattered field calculation in heterogeneous media using a phase-screen propagator: SEG Technical Program Expanded Abstracts, **11**, 1289–1292.